Macromolecules
ARTICLE

Macromolecules **2010**, *43*, 10521–10527 **10521**
DOI: 10.1021/ma102500w

Field-Induced Transport in Sulfonated Poly(styrene-*co*-divinylbenzene) Membranes

Oscar Bertran,*,† David Curcó,‡ Juan Torras,§ Carlos A. Ferreira,⊥ and Carlos Alemán*,∥,○

†*Departament de Física Aplicada, EEI, Universitat Politècnica de Catalunya, Pça. Rei 15, 08700 Igualada, Spain,* ‡*Department d'Enginyeria Química, Facultat de Química, Universitat de Barcelona, Martí Franques 1, Barcelona E-08028, Spain,* §*Departament d'Enginyeria Química, EEI, Universitat Politècnica de Catalunya, Pça. Rei 15, 08700 Igualada, Spain,* ⊥*Universidade Federal do Rio Grande do Sul, PPGEM, Av. Bento Gonçalves, 9500, setor 4, prédio 74, Cep. 91501-970, Porto Alegre, RS, Brazil,* ∥*Departament d'Enginyeria Química, E. T. S. d'Enginyers Industrials, Universitat Politècnica de Catalunya, Diagonal 647, 08028 Barcelona, Spain, and* ○*Center for Research in Nano-Engineering, Universitat Politècnica de Catalunya, Campus Sud, Edifici C', C/Pasqual i Vila s/n, Barcelona E-08028, Spain*

Received November 3, 2010; Revised Manuscript Received November 23, 2010

ABSTRACT: Atomistic simulations have been carried to investigate electric field induced transport of hydronium ions in a sulfonated poly(styrene-*co*-divinylbenzene) membrane. In order to provide a good description of this cross-linked material, a methodology has been explicitly designed to construct a reliable model of the hydrated membrane. This model has been used to carry out molecular dynamics simulations in presence of electric fields, which varied from 0.001 to 3.0 $V \cdot nm^{-1}$. Results show that the electric field affects the structure of the membrane producing both a redistribution of the unoccupied volume, which modifies the heterogeneity of the resin, and a rearrangement of the negatively charged sulfonate groups, which undergo a systematic alignment along the electric field direction. As was expected, the mobility of hydronium ions is enhanced with the strength of the electric field. Moreover, the electric field induces a significant rearrangement of the sulfonate groups, which is evidenced by the alignment of the C−S bonds along the direction of the field. The membrane has been found to behave as a spring, in which the force exerted by the electric field acts in opposite sense to the force exerted by the internal structure of the cross-linked material.

Introduction

Ion-exchange membranes play an important role in an increasing number of processes in chemical industry. For example, they are used in electrodialysis and as separators in electrolytic cells and fuel cells.[1−3] According to their structure, commercial ion-exchange membranes can be divided into homogeneous ones, which are constituted by cross-linked polymers having ion-exchange groups bound to the polymer backbone, and into heterogeneous ones, which consist of a neutral polymeric matrix filled with ion-exchange microparticles.[4,5]

Polymeric resins based on poly(styrene-*co*-divinylbenzene), hereafter denoted P(S-DVB), are employed to prepare cation-exchange homogeneous membranes by functionalizing with sulfonic acid groups.[6−10] Thus, sulfonated P(S-DVB)-based membranes have been stated to be the best for use in electrodialysis because the cross-linked polystyrene has more phenyl rings that act as reactive sites for functionalization reactions like sulfonation.[4] In the production of these membranes, which are commercial (e.g., CR61-CZL-412 produced by Ionics Inc.), styrene and divinylbenzene (DVB) are copolymerized in aqueous solution using an initiator to get a homogeneous polymer solution, DVB acting as a cross-linking agent. Then, the cation-exchange membranes are prepared by the sulfonation of polymer in solution with concentrated sulfuric acid in dichloroethane.

The investigation of transport and equilibrium phenomena in ion-exchange membranes have been studied in a number of papers,[11−14] and additionally, some mathematical models have been proposed to explain the macroscopic characteristics of such processes (e.g., proton transport and membrane conductivity).[15−17] However, in spite of such significant amount of work, nanoscale details about the molecular structure of ion-exchange membranes and the proton transport mechanism remain essentially unknown. Although theoretical studies based on molecular dynamics (MD) simulations are expected to be important not only for the elucidation of details about the protons transport across membranes but also for the design of good performance conducting membranes, the number of reported investigations is relatively scarce.[18−24] Goddard and co-workers used atomistic MD simulations to predict the nanostructure of hydrated Nafion 117, a polyelectrolyte consisting of nonpolar tetrafluoroethylene and polar perfluorosulfonic vinyl ether segments used in polymer electrolyte membrane fuel cells, with a focus on investigating the effect of the polar and nonpolar monomeric sequence on the nanophase-segregated morphology and the water/hydronium transport.[18] More recently, the effects of electric field in transport dynamics inside hydrated Nafion membranes were investigated by different authors.[19−22] In addition, Allahyarov and Taylor[23] used MD simulations to investigate the effect of stretching induced structure on the proton conductivity of Nafion-like polymer electrolyte membranes. Results showed that uniaxial stretching causes the hydrophilic regions to become elongated in the stretching direction, enhancing the conductivity along such direction. Riande and co-workers simulated the diffusion of naked and hydrated protons across sulfonated poly(phenyl sulfone)s.[24] The chemical model used by these authors to represent the

*Corrsponding authors. E-mail: (O.B.) oscar.betran@upc.edu; (C. A.) carlos.aleman@upc.edu.

Published on Web 12/06/2010

membrane was very simple (i.e., a cell containing five chains of 10 repeating units), the simulated conductivities obtained for the hydrated proton being roughly similar to the experimentally measured ones. In spite of this, simulations described very satisfactorily the Arrhenius behavior of the proton conductivity.

In spite of the increasing interest for electrodialysis, nanoscale details about the transport process inside of sulfonated P(S-DVB) soft membranes have not been reported yet. It should be noted that the cross-linked nature of this material makes difficult the application of conventional methods to obtain reliable starting models at the molecular level. In this work atomistic MD simulations have been performed on a realistic system to provide nanoscale understanding of the hydronium transport in sulfonated P(S-DVB) membranes at the molecular level. For this purpose, a molecular model for the resin support was constructed using an explicitly designed methodology and, subsequently, hydrated and equilibrated. After this, external electric fields ranging from 0.001 to 3.0 $V \cdot nm^{-1}$ were used to examine both the transport of hydronium ions across the membrane and the relationship with the structure of this support.

Methods

The energy of the simulated system was calculated in all cases using the following analytical potential function:

$$E = \sum_{angles} k_b(\theta - \theta_0)^2 + \sum_{dihedrals} \sum_{n=1}^{3} \frac{V_n}{2}[1 + \cos(n\phi - \gamma)] + \sum_{improper} k_i(\varphi - \varphi_0)^2 \sum_{nonbonded} \left\{ 4\sqrt{\varepsilon_i \varepsilon_j} \left[\left(\frac{\sigma_i + \sigma_j}{r_{ij}} \right)^{12} - \left(\frac{\sigma_i + \sigma_j}{r_{ij}} \right)^{6} \right] + \frac{q_i q_j}{R_{ij}} \right\} \quad (1)$$

The first sum represents the bending of the bond angles, the second term corresponds to a series expansion for the torsional term that has been applied to the flexible bonds of the backbone, the third contribution refers to the deformation of the improper torsions and, finally, the last sum describes the van der Waals and electrostatic interactions (i.e., nonbonding energy contributions). Atoms and pseudoatoms of sulfonated P(S-DVB) has been classified according to 11 atoms types (Figure S1 of the Supporting Information), four additional types being used to categorize the atoms of the water and hydronium molecules. As it can be seen, a united atom model (i.e., pseudoatoms) rather than the all atom one has been used describe carbon and hydrogen atoms directly bonded.

Force-field parameters are for P(S-DVB) were extrapolated from the TraPPE united atom force-field for polystyrene[25] and from the general AMBER force-field (GAFF),[26] those of the sulfate groups were taken from GAFF,[26] whereas water and hydronium molecules were described using the TIP3P[27] and the Baadem et al.[28] models, respectively. A complete description of the force-field parameters is provided in the Supporting Information (Tables S1−S3). The molecular geometry of the water (bond lengths and bond angle) and hydronium (bond lengths, bond angles, and improper torsion) molecules were kept fixed during the whole MD simulations.

MD simulations were performed using the DLPOLY 2.19 program.[29] Atom pair distance cutoffs were applied at 14.0 Å to compute the van der Waals interactions. Electrostatic interactions were computed using the nontruncated electrostatic potential with Ewald summations.[30] The real space term was determined by the van der Waals cutoff (14.0 Å), while the reciprocal term was estimated by interpolation of the effective charge into a charge mesh with a grid thickness of five points per volume unit (i.e., the particle-mesh Ewald, PME, method).[30] Bond lengths were constrained using the SHAKE algorithm,[31] and the numerical integration step was set to 2 fs. Both temperature and pressure were controlled by the weak coupling method, the Berendsen thermo-barostat,[32] using a time constant for the heat bath coupling and a pressure relaxation time of 1 ps.

An external electric field fixed along the z-axis of the simulation, with values ranging from $\vec{E}_z = 0.001$ $V \cdot nm^{-1}$ to $\vec{E}_z = 3.0$ $V \cdot nm^{-1}$, was used as driven force box for the hydronium transport process. Accordingly, the force on an atom i ($\vec{F}'_i$) was defined through the following expression:

$$\vec{F}'_i = \vec{F}_i + q_i \vec{E}_z \quad (2)$$

where $\vec{F}_i$ is the force defined by the interaction potential provided in eq 1 and q_i is the charge of the atom.

Results and Discussion

Construction, Hydration, and Equilibration of the Membrane. Construction of heterogeneously ordered macromolecular multichain systems is very unpractical because the relatively high density and the connectivity of the molecular systems reduce significantly the efficiency of conventional simulation methods.[33,34] In addition, the construction of the P(S-DVB) membrane is also restricted by the cross-links formed by the DVB units. In order to overcome these difficulties, a new approach based on other strategies recently reported for simple amorphous polymers[34−36] has been developed and subsequently used. This approach, which is described with more detail in the Supporting Information, can be summarized in the following four steps (Figure 1):

(1) *Selection of the Molecular Architecture*. The generation has been performed considering pseudounits (Figure 1a) formed by 10 pseudoatoms in the main chain and the five corresponding phenyl groups. The position of the pseudoatoms contained in the first pseudounit are generated within the simulation box using algorithms that were previously designed to provide conformations with minimum torsional strain and without repulsive nonbonding interactions for conventional amorphous polymers.[35−37] The position to grow the second pseudounit is selected among three options (Figure 1a) using a Monte Carlo (MC) criterion: (i) the second pseudounit is bounded to the right side of the first one; (ii) the second pseudounit is bounded to the left side of the first one; and (iii) the second pseudounit is attached to one of the five phenyl rings of the first pseudounit forming a cross-link.

(2) *Construction of the New Pseudounit*. If option iii was chosen in the previous step, both a ring of the first pseudounit and a pseudoatom of the main chain of the second unit are randomly chosen to form a cross-link. The cross-link is considered as feasible when steric overlaps with previously generated pseudoatoms do not occur, whereas two new elements involved in the formation of the cross-link are selected again if steric overlaps are detected. If the option selected in step 1 was option i or ii, the first or tenth pseudoatom of the main chain of the second pseudounit is randomly chosen, and the possible existence of steric overlaps is examined. If necessary, the chosen pseudoatom is changed to avoid steric clashes. Independently of the molecular architecture, the positions of the pseudoatom contained the pseudounit are obtained one-by-one.

(3) *Repetition of the Process*. The rest of the pseudounits are generated one-by-one using the same procedure.

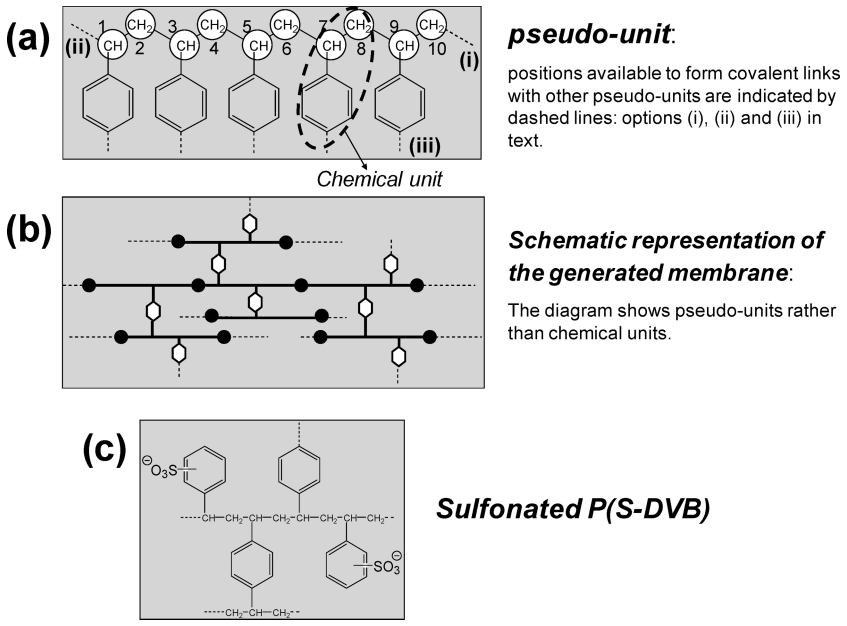

Figure 1. Schematic representation of the main steps involved in the construction of the P(S-DVB) microstructures: (a) definition of the pseudounit used in the generation process, which is constituted by ten chemical units, as well as of the positions (dashed lines) used to grow the membrane (options i, ii, and iii in the text); (b) generated system, including the cross-links; and (c) chemical structure of the sulfonated P(S-DVB).

Some distinctive features of this repetition process are as follows: (a) the new pseudounit can be linked to any of the previously generated pseudounits; and (b) there is no restriction in the number of cross-links associated with every pseudounit, even though the concentration of cross-links must be equal to the concentracion of DVB units at the end of the generation process. The generated membrane is schematically represented in Figure 1b.

(4) *Sulfonation*. Sulfonic acid groups are introduced one-by-one (Figure 1c). For this purpose, one phenyl ring and, subsequently, one of its available free positions are randomly chosen. If the added sulfonic acid group does not present steric overlaps, the generated position is accepted.

This algorithm has been used to construct 100 microstructures of sulfonated P(S-DVB) considering a cubic simulation box of dimensions a = 97.83 Å (ρ = 0.64 g·cm^{-3}), which contains 2165 styrene units, 270 DVB units and 1294 sulfonic acid groups. The energy of all the generated microstructures was initially minimized to relax conformational and structural tensions using the conjugate gradient method for 5 × 10^3 steps. After this, the five microstructures of lower energy were hydrated. This was performed by applying an algorithm able to detect very efficiently the unoccupied volume (i.e., the empty space accessible to a given penetrant molecule) in polymeric matrices.[38] The size of the penetrant used to localize the unoccupied volume within each microstructure was defined by the van der Waals radius of the oxygen atom (R = 1.77 Å). A total of 4750 water molecules (19.3% w/w) were randomly introduced in each microstructure at positions identified as unoccupied. From these water molecules, 1294 were randomly chosen and transformed into hydronium ions to reach the neutrality of the system. Accordingly, the final composition (in % w/w) of the simulated membrane was: 50.8% of styrene units, 6.3% of DVB units, 23.3% of sulfonic acid groups, 14.0% of water molecules and 5.5% of hydronium ions.

After energy minimization, the hydrated microstructures were subjected to 50 ps of NVT−MD at 300 K to relax the system. The final snapshot of lowest energy was selected as starting point for equilibration and production runs. In this system, whose chemical complexity is reflected in Figure 2, the sulfonic acid groups were distributed as follows: 1255 (97%) were directly linked to styrene units, while only 39 were located in DVB units. Initially, in order to equilibrate the system, different consecutive rounds of short MD runs were performed. First, 10 ps of NVT−MD at 500 K were used to distribute homogeneously the particles in the simulation box. Second, 10 ps of isobaric relaxation were run. Finally, the system was submitted to 15 ps of steady heating

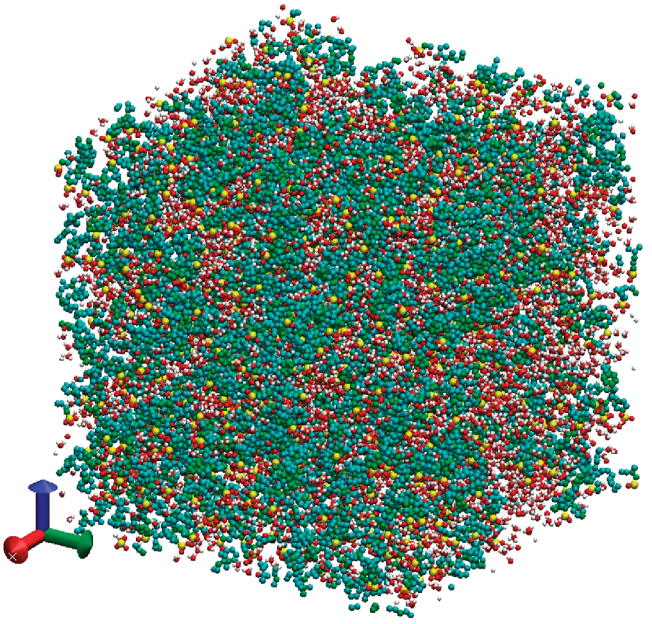

Figure 2. Schematic representation of the simulation box. Aliphatic CH and CH_2 pseudoatoms are indicated in blue, while the CH of the phenyl rings are depicted in green. The sulfur (sulfonic acid groups), oxygen (sulfonic acid, water molecules, and hydronium ions) and hydrogen (water molecules and hydronium ions) atoms are represented in yellow, red, and white, respectively.

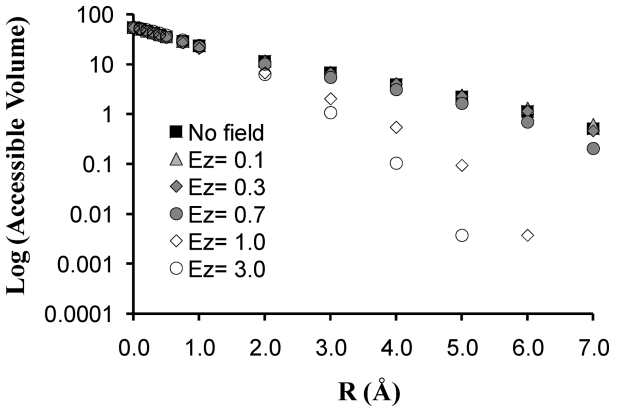

Figure 3. Logarithmic variation of the accessible volume to a given spherical penetrant (unoccupied volume, in %) against the radius of the penetrant (R) for sulfonated P(S-DVB). The accessible volume has been determined using the microstructures provided by MD simulations in absence and presence of selected electric fields (E_z = 0.1, 1.0, and 3.0 V·nm^{-1}). Water and hydronium molecules have not been considered for the evaluation of the accessible volume.

until the target temperature (300 K) was reached, 10 ps of NVT−MD at 300 K (thermal equilibration), followed by 10 ps of density relaxation (NPT−MD). After equilibration, a 3 ns production run was performed in absence of electric field.

In order to examine the influence of the relaxation and equilibration protocol in the properties and dynamics of sulfonated P(S-DVB), different procedures were examined. These differ in the length of the MD run used for relaxation (NVT−MD, which ranged from 5 to 250 ps, and those used for equilibration (both NVT− and NPT−MD), which ranged from 5 to 35 ps. In all cases results (i.e., structure, density, accessible volume, etc.) were practically identical to those described below. For example, the largest variation of the density amounts to 4.5% only. These similarities should be attributed to effect of the cross-links, which restricts the flexibility of the sulfonated P(S-DVB) minimizing the influence of the protocol on the properties of the material.

The most remarkable characteristic of the sulfonated P(S-DVB) membrane is its high porosity, this structural feature being also detected in each of the 100 microstructures constructed and relaxed using the procedure described above. Thus, although no restriction was introduced in the generation algorithm and the minimization process, the distribution of pseudoatoms in the resulting microstructures was heterogeneous rather than homogeneous as expected. This is reflected in Figure 3 for snapshots recorded during the production MD run, which represents the unoccupied volume (i.e., the volume accessible to a spherical penetrant of radius R). An approximated straight line until a given radius followed by a sharp decay should be expected for homogeneous microstructures. In contrast, Figure 3 also indicates that the unoccupied volume decreases progressively when R increases, evidencing a heterogeneous distribution of pores in the material.

Effect of the Electric Field. The last snapshot of the trajectory in absence of electric field was used as starting point for nine independent MD simulations in presence of the following electric fields: 0.001, 0.01, 0.03, 0.1, 0.3, 0.7, 1.0, 2.0, and 3.0 V·nm^{-1}. Electric fields were fixed along the z-axis of the simulation box, each trajectory being 3 ns long and the coordinates were saved every 10 ps.

Figure 4a displays the average density of the system against the strength of the electric field, while Figure 4b represents the temporal evolution of this property. As it can

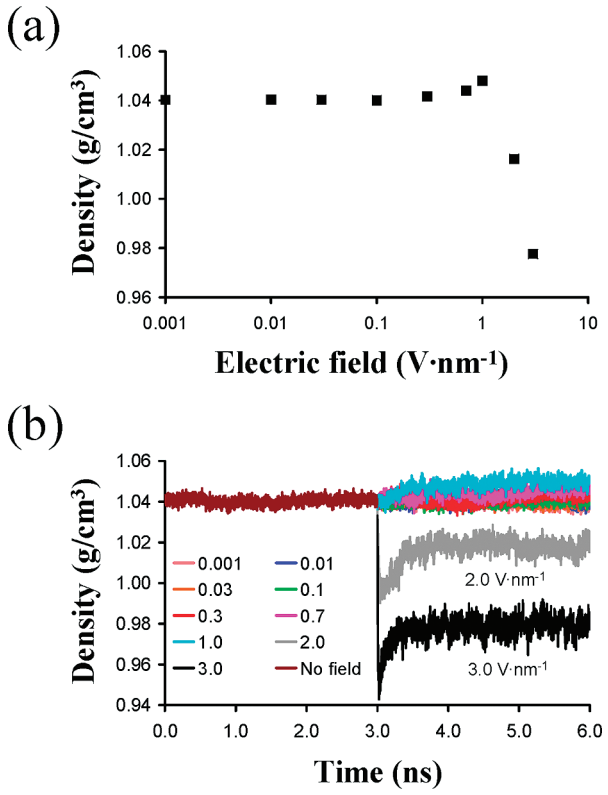

Figure 4. (a) Variation of the average density against the electric field and (b) temporal evolution of the density obtained considering $\vec{E}_z$ = 0.001, 0.01, 0.03, 0.1, 0.3, 0.7, 1.0, 2.0, and 3.0 V·nm^{-1}.

be seen, the structure of the material remains practically unaltered until $\vec{E}_z$ = 1.0 V·nm^{-1}, the density decreasing above such electric field. Inspection of the different energy contributions indicate that such variations, which amount to 2% and 6% for 2.0 and 3.0 V·nm^{-1}, cannot be attributed to the deformation of the internal geometry (i.e., bond lengths and angles) produced by $\vec{E}_z$. Figure 3, which shows the variation of the unoccupied volume obtained in presence of selected electric fields, indicates that the volume accessible to penetrants larger than ∼1 Å decreases with respect to that obtained in absence of electric field when $\vec{E}_z \geq$ 2.0 V·nm^{-1}. Thus, such high electric fields tend to reduce the heterogeneity detected for the unperturbed membrane, even though it remains practically unaltered upon the application of for lower $\vec{E}_z$ (Figure S2, Supporting Information). As will be showed below, the variation of the unoccupied volume and the density are consequence of important local rearrangements undergone by the charged sulfonate groups in presence of such high electric fields. Results displayed in Figure 4b reflect that the convergence of the density is very fast, independently of the strength of the electric field.

A more detailed examination of the influence of the electric field in the structure of the membrane reveals a deformation due to a rearrangement of the sulfonate groups, which starts at 0.3 V·nm^{-1}. This is evidenced in Figure 5a, which shows the temporal average value of the averaged projection of the C−S bond into the z-axis (p_z^{CS}), i.e. in the direction of the electric field. As it was expected, p_z^{CS} is zero in absence of electric field, which indicates that the arrangement of the sulfonate groups in the membrane follows a random distribution. However, p_z^{CS} increases with the electric field. Although such increment is relatively low for electric fields ranging from 0.001 to 0.1 V·nm^{-1}, it is very significant after 0.3 V·nm^{-1}, as it reflects the value reached

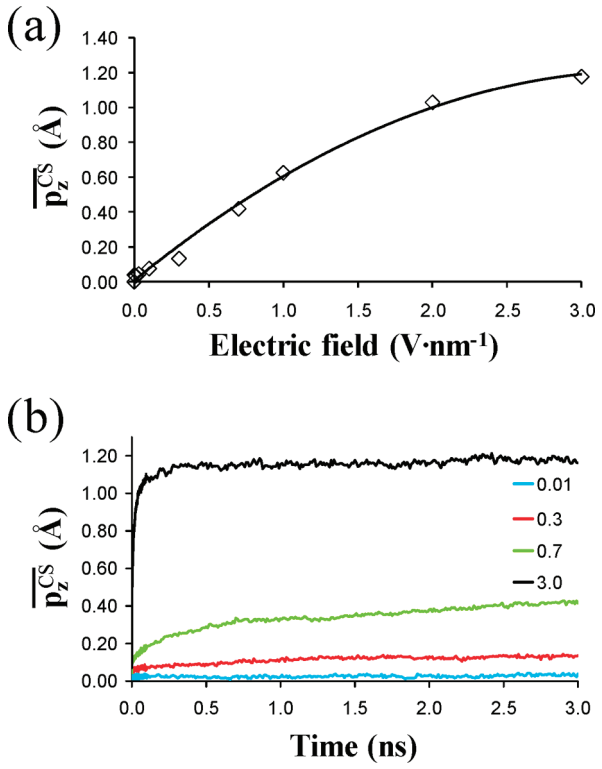

Figure 5. (a) Variation of the temporal average value of the averaged projection of the C−S bond into the z-axis ($\overline{p_z^{CS}}$) against the electric field. (b) Temporal evolution of $\overline{p_z^{CS}}$ for selected electric fields, which are represented using different colors.

at 3.0 V·nm^{-1} ($\overline{p_z^{CS}}$ = 1.178 Å). Thus, the sulfonate groups undergo a drastic rearrangement, which consists in the alignment of C−S bonds along the direction of the electric field. This behavior is identical to that typically observed in polar dielectrics under the action of an external electric field, where their dipole moments are aligned with the electric field.[39]

Inspection of the temporal evolution of $\overline{p_z^{CS}}$ for selected electric fields, which is displayed in Figure 5b, indicates that the rearrangement of the sulfonate groups occurs progressively for moderate electric fields (i.e., ≤3.0 V·nm^{-1}), the overall process taking around 2 ns. In contrast, for the highest electric field the deformation of the membrane takes place in the first stages of the simulation (i.e., the rearrangement of the sulfonate groups is completed after ∼0.4 ns). Results displayed in Figure 5 allows one to explain the variation of the unoccupied volume and the density against the electric field (Figures 3 and 4, respectively). Thus, the rearrangement of the sulfonate groups produces the swelling of the membrane (i.e., the density decreases) and the redistribution of the accessible volume (i.e., unoccupied volume for penetrants with R > 1 Å decreases.

In order to analyze the average velocity of the hydronium ions in presence of an electric field, the last 2 ns of each trajectory was divided in 40 snapshots separated by 50 ps. Figure 6a represents for selected electric fields the variation of the number of hydroniums (N_{ions}) against the distance covered in the simulation box during 50 ps (Δ_{50}) when $\Delta_{50} \geq$ 0.4 Å. In general about 50% of the total hydronium ions (i.e., the latter is 1294 explicit H_3O^+ in the simulation box × 40 snapshots = 51760) moved less than 0.4 Å when the electric field was higher than 0.3 V·nm^{-1}, such amount increasing to 75% for lower electric fields. The velocity of ions is directly related with the strength of the electric field, both exponential and linear behaviors being detected in Figure 6a. For electric

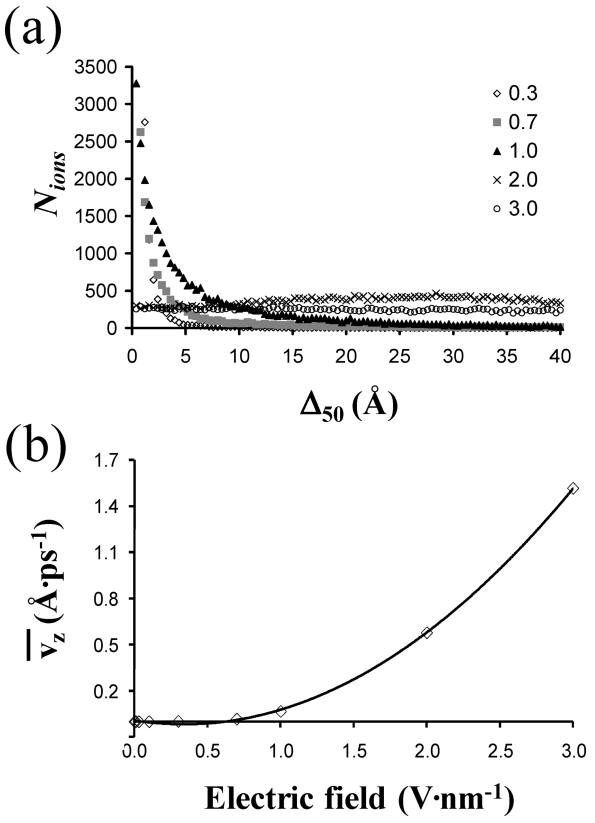

Figure 6. (a) For selected electric fields, variation of the number of hydronium ions (N_{ions}) against the distance covered in the simulation box during 50 ps (Δ_{50}) when $\Delta_{50} \geq$ 0.4 Å. (b) Variation of the average velocity of the hydronium ions along the z-axis ($\overline{V_z}$) against the electric field.

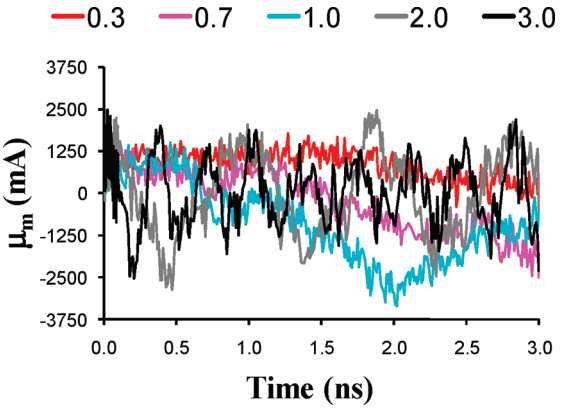

Figure 7. Temporal evolution of the membrane dipole moment (μ_m) considering different electric fields (in V·nm^{-1}), which are represented using different colors.

fields lower than 2.0 V·nm^{-1} N_{ions} decays exponentially when Δ_{50} increases, independently of the number of ions with $\Delta_{50} \geq$ 0.4 Å. Thus, the number of hydronium able to cover small distances in 50 ps is high, whereas a reduced number of ions moves large distances in such small period of time. In opposition, the variation of N_{ions} against Δ_{50} follows a linear behavior for 2.0 and 3.0 V·nm^{-1}, reflecting that the number of hydroniums covering distances of 0.4 and 16.0 Å is approximately the same at such high electric fields.

Figure 6b represents the average velocity of the hydronium ions along the direction of the electric field (V_z) against the own electric field. It should be noted that results are fully

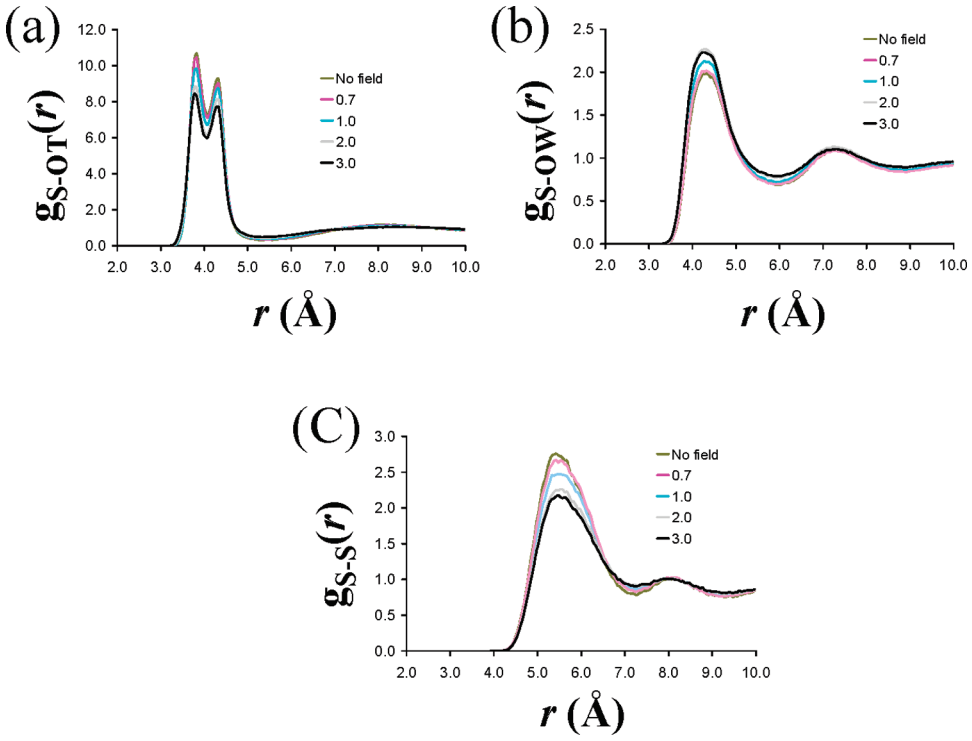

Figure 8. Partial distribution functions of (a) S···OT, (b) S···OW, and (c) S···S pairs for selected electric fields, which are represented using different colors.

consistent with those showed in Figure 6a. Thus, $\overline{V_z}$ is practically null (i.e., lower than 0.001 Å·ps^{-1}) for electric fields lower than 0.3 V·nm^{-1} increasing slowly but progressively until the electric reach a value of 1.0 V·nm^{-1}. After this the velocity increases sharply reaching a value of $\overline{V_z}$ = 1.52 Å·ps^{-1} when the electric field is 3.0 V·nm^{-1}. The transport of the hydronium ions across the membrane is illustrated in the Supporting Information, which includes a movie showing the move the selected ions during the trajectory.

In order to show the strain exerted by the electric field in the membrane, the temporal evolution of the dipole moment (μ_m) has been depicted in Figure 7. It should be remarked that hydronium ions and water molecules were excluded from the calculation of μ_m. The oscillations observed for the higher electric fields evidence that the membrane behaves as a spring, which is due to the balance between the strength exerted by the electric field and the strength associated with the structure of the membrane. As a consequence, the oscillatory behavior of μ_m presents a relatively low frequency (i.e., about 1 ns for the 3.0 V·nm^{-1} simulation). However, the deformation of the structure becomes more difficult when the strength of the electric field decreases, producing an increase of the oscillatory frequency. Indeed, the length of the simulation is too short to detect the spring behavior for electric fields lower than 0.1 V·nm^{-1}.

Parts a and b of Figure 8 show the partial radial distribution functions, $g_{ij}(r)$, of the S···OT and S···OW pairs (where OT and OW refer to the oxygen hydronium and water molecules, respectively, as is indicated in the Supporting Information) for selected electric fields. The $g_{S\text{-}OT}(r)$ function shows two pronounced sharp peaks centered at 3.8 and 4.3 Å in all cases, including that without electric field. However, the height of such peaks decreases when the strength of the electric field increases, the reduction being particularly remarkable for 2.0 and 3.0 V·nm^{-2}. This change is accompanied by a subtle but detectable redistribution of the S···OT pairs located between 5 and 7 Å. Thus, the number of pairs in this region increases with the strength of the electric field demonstrating the influence of the latter in the local structure of the sulfonate groups. Similar trends are observed in the $g_{S\text{-}OW}(r)$ function, even though in this case the two pronounced peaks are broad and centered at 4.2 and 7.2 Å. The height of such peaks diminishes when the strength of the electric increases, causing an enlargement in the number of S···OW pairs in the region comprised between 5 and 7 Å. These results allow us conclude that the local structural distortions induced by the electric fields are similar for all the sulfonated groups, independently of the surrounding environment. Figure 8c, which presents the partial radial distribution function of the S···S pairs, indicates that the membrane present local order in absence of electric field and in presence of small electric fields. This is reflected by the pronounced broad peak at 5.4 Å and the small broad peak at 8.0 Å. However, the local order is removed upon the application of high electric field, as is evidenced the by the disappearance of the second peak.

Conclusions

A new computational strategy for the generation and relaxation of cross-linked systems has been developed. This methodology has been used to prepare 100 atomistic microstructures of sulfonated P(S-DVB), which have been considered as starting points of MD simulations in absence and presence external electric fields. Analyses of the recorded trajectories indicate that application of an electric field affects the structure of sulfonated P(S-DVB). These effects, which are particularly evident when the strength of the electric field surpasses a given threshold value ($E_z \approx$ 1.0 V·nm^{-1}), mainly refer to the homogeneity of the membrane and the arrangement of the sulfonate groups. Thus, analysis of the distribution of the accessible volume indicate that the homogeneity of the membrane increases with the strength of electric field, while the C−S bond of the sulfonate groups tends to align along the direction of the electric field.

Membranes made of sulfonated P(S-DVB) show a particular spring-like behavior upon the action of an external electric field, which should be attributed to the cross-linked nature of this material. Thus, the electric field tends to alter the structure of the membrane straining it in the direction and sense of the field, whereas DVB cross-links exert a force in the same direction but opposite sense. The balance between such two forces is responsible of the oscillatory behavior detected for μ_m, in which the frequency decreases when the strength of the electric field increases.

As it was expected, the mobility of the hydronium ions increases with the strength of the electric field. This is reflected by the average velocity of the ions, which increases from $\sim 10^{-5}$ Å·ps^{-1} to 1.52 Å·ps^{-1} when the electric field changes from 0.001 V·nm^{-1} to 3.0 V·nm^{-1}. Furthermore, the distribution of ions with high mobility is also influenced by the strength of the electric field. Thus, for low and moderate electric fields the variation of the number of ions against the covered distance follows an exponential behavior (i.e., the number of ions covering small distances is significantly higher than the number of ions showing large displacements). In contrast, a linear behavior has been found for large electric fields (i.e., the number of ions covering small and large distances is similar).

Acknowledgment. This work has been supported by MICINN and FEDER (Grants MAT2009-09138 and PHB2007-0038-PC), by the Generalitat de Catalunya (research group 2009 SGR 925 and XRQTC) and by CAPES-MICINN International Cooperation Program from Brazilian and Spanish Education and Science Ministries. Computer resources were generously provided by the "Centre de Supercomputació de Catalunya" (CESCA). Support for the research of C.A. was received through the prize "ICREA Academia" for excellence in research funded by the Generalitat de Catalunya.

Supporting Information Available: Tables and figures giving a detailed description of the force-field parameters (van der Waals, electrostatic, bending and torsion), description of the atom types and variation of the accessible volume against the size of the penetrant and a movie to illustrate the transport of hydronium ions. This material is available free of charge via the Internet at http://pubs.acs.org.

References and Notes

(1) Prakash, P.; Hoskins, D.; SenGupta, A. K. *J. Membr. Sci.* **2004**, *237*, 131.
(2) Larchet, C.; Eigenberger, G.; Tshkay, A.; Tastanov, K.; Nikonenko, V. *Desalination* **2002**, *149*, 383.
(3) Wee, J. H. *Renew. Sustain. Energy Rev.* **2007**, *11*, 1720.
(4) Kariduraganavar, M. Y.; Nagarale, R. K.; Kittur, A. A.; Kulkarni, S. S. *Desalination* **2006**, *197*, 225.
(5) Volodina, E.; Pismenskaya, N.; Nikonenko, V.; Larchet, C.; Pourcelly, G. *J. Colloid Interface Sci.* **2005**, *285*, 247.
(6) Abrams, I. M.; Benezra, L. In *Encyclopedia of Polymer Science & Technology*; Frank, M. H., Bikales, N. M., Overberg, C. G., Menges, G., Eds.; John Wiley: New York, 1965; Vol. *7*, pp 693−731.
(7) Okay, O. *Prog. Polym. Sci.* **2000**, *25*, 711.
(8) Coutinho, F. M. B.; Rezende, S. M.; Soares, B. G. *J. Appl. Polym. Sci.* **2006**, *102*, 3616.
(9) Tuan, L. X.; Hanae, B.; Vargas-Lara, M.; Claudine, B.-H. *Electrochim. Acta* **2009**, *54*, 5992.
(10) Tiihonen, J.; Laatikainen, Markkanen, I.; Paatero, E. *Ind. Eng. Chem. Res.* **1999**, *38*, 4832.
(11) Choi, J. H.; Kim, S. H.; Moon, S. H. *J. Colloid Interface Sci.* **2001**, *241*, 120.
(12) Majsztrik, P. W.; Satterfield, M. B.; Bocarsly, A. B.; Benziger, J. B. *J. Membr. Sci.* **2007**, *301*, 93.
(13) Kujawski, W.; Staniszewski, M.; Nguyen, T. Q. *Sep. Purif. Technol.* **2006**, *57*, 476.
(14) Nagarale, R. K.; Gohil, G. S.; Shahi, V. *Adv. Colloid Interface Sci.* **2006**, *119*, 97. (b) Xu, T. *J. Membr. Sci.* **2005**, *263*, 1.
(15) Gnusin, N. P.; Berezina, N. P.; Kononenko, N. A.; Dyomina, O. A. *J. Membr. Sci.* **2004**, *243*, 301.
(16) Berezina, N. P.; Kononenko, N. A.; Dyomina, O. A.; Gnusin, N. P. *Adv. Colloid Interface* **2008**, *139*, 3.
(17) Pisani, L.; Valentini, M.; Hofmann, D. H.; Kuleshova, L. N.; D'Aguanno, B. *Solid State Ionics* **2008**, *179*, 465.
(18) Jang, S. S.; Molinero, V.; Cagin, T.; Goddard *J. Phys. Chem. B* **2004**, *108*, 3149.
(19) Chen, P. Y.; Hong, C. W. *Fuel Cells* **2010**, *10*, 17.
(20) Allahyarov, E.; Taylor, P. L.; Lowen, H. *Phys. Rev. E* **2010**, *81*, 031805.
(21) Shao, S.; Yan, L.; Zhu, S.; Zhu, S. *J. Chem. Phys.* **2009**, *131*, 224901.
(22) Yan, L.; Ji, X.; Lu, W. *J. Phys. Chem.* **2008**, *112*, 5602.
(23) Allahyarov, E.; Taylor, P. L. *J. Phys. Chem. B* **2009**, *113*, 610.
(24) Pozuelo, J.; Riande, E.; Saiz, E.; Compañ, V. *Macromolecules* **2006**, *39*, 8862.
(25) Wick, C. D.; Martin, M. G.; Siepmann, J. I. *J. Phys. Chem. B* **2000**, *104*, 8008.
(26) Wang, J.; Wolf, R. M.; Caldwell, J. W.; Kollman, P. A.; Case, D. A. *J. Comput. Chem.* **2004**, *25*, 1157.
(27) Jorgensen, W. L.; Chandrasekhar, J.; Madura, J. D.; Impey, R. W.; Klein, M. L. *J. Chem. Phys.* **1983**, *79*, 926.
(28) Baaden, M.; Burgard, M.; Wipff, G. *J. Phys. Chem. B* **2001**, *105*, 11131.
(29) http://www.cse.scitech.ac.uk/ccg/software/DL_POLY/index.shtml
(30) Darden, T.; York, D.; Pedersen, L. *J. Chem. Phys.* **1993**, *98*, 10089.
(31) Ryckaert, J. P.; Ciccotti, G.; Berendsen, H. J. C. *J. Comput. Phys.* **1977**, *23*, 327.
(32) Berendsen, H. J. C.; Postma, J. P. M.; van Gunsteren, W. F.; DiNola, A.; Haak, J. R. *J. Chem. Phys.* **1984**, *81*, 3684.
(33) Leontidis, E.; Forrest, B.; Widmann, A. H.; Suter, U. W. *J. Chem. Soc., Faraday Trans.* **1995**, *91*, 2355.
(34) Alemán, C.; Karayiannis, N. Ch.; Curcó, D.; Foteinopoulou, K.; Laso, M. *J. Mol. Struct.* (*Theochem*) **2009**, *898*, 62.
(35) Curcó, D.; Alemán, C. *J. Chem. Phys.* **2003**, *119*, 2915.
(36) Curcó, D.; Alemán, C. *J. Comput. Chem.* **2004**, *25*, 790.
(37) Curcó, D.; Alemán, C. *J. Comput. Chem.* **2007**, *28*, 1743.
(38) Curcó, D.; Zanuy, D.; Alemán, C. *J. Comput. Chem.* **2003**, *24*, 1208.
(39) Vanderlinde, J. *Classical Electromagnetic Theory*; Springer: Berlin, 2004; p 165.